RESEARCH ARTICLE | JUNE 27 2023

# Light soaking effects on full-area and half-cut silicon heterojunction solar cells FREE

Sebastian Pingel ✉; Anamaria Steinmetz; Martin Bivour; Sebastian Roder; Ioan Voicu Vulcanean; Karin Zimmermann; Winfried Wolke; Vasileios Georgiou-Sarlikiotis; Leonard Tutsch; Timo Wenzel; Denis Erath; Andreas Lorenz; Anna Münzer; Puzant Baliozian; Armin Richter; Torsten Rößler; Esther Fokuhl; Paul Gebhardt; Jochen Rentsch; Jale Schneider; Florian Clement; Jan Nekarda; Ralf Preu



*AIP Conference Proceedings* 2826, 090004 (2023)
https://doi.org/10.1063/5.0141313

# Light Soaking Effects on Full-Area and Half-Cut Silicon Heterojunction Solar Cells

Sebastian Pingel[a)], Anamaria Steinmetz, Martin Bivour, Sebastian Roder, Ioan Voicu Vulcanean, Karin Zimmermann, Winfried Wolke, Vasileios Georgiou-Sarlikiotis, Leonard Tutsch, Timo Wenzel, Denis Erath, Andreas Lorenz, Anna Münzer, Puzant Baliozian, Armin Richter, Torsten Rößler, Esther Fokuhl, Paul Gebhardt, Jochen Rentsch, Jale Schneider, Florian Clement, Jan Nekarda and Ralf Preu

*Fraunhofer Institute for Solar Energy Systems (ISE), Heidenhofstraße 2, 79110 Freiburg, Germany*

[a)] Corresponding author: sebastian.pingel@ise.fraunhofer.de



**Abstract.** Lightsoaking (LS) of n-type silicon heterojunction (SHJ) solar cells is a topic that raised increasing attention of the PV industry. The treatment of n-type SHJ with high light intensity and high temperature in parallel leads to a boost in efficiency (η) that is driven by improved passivation at open-circuit and MPP ($V_{oc}$, pFF) and reduced series resistance ($R_S$), both together leading to a higher FF of the cell. Within this paper we investigate the effects of LS and show that LS can be an effective means to modify and improve layer and interface properties. However, to fully take advantage and maximize η the post processing by LS and the individual cell / module processing steps must be well aligned. Here we show that transparent conductive oxide (TCO) deposition conditions can have a significant influence for a given LS treatment. Furthermore, we combine the LS treatment with cell separation and edge passivation technology, the so-called post processing of the cell to overcome losses resulting from separation of half-cut (HC) SHJ cells. Further, we demonstrate that SHJ cells were successfully separated with low η loss applying a slim post processing sequence. From these cells a monofacial and a bifacial module were built and characterized. Finally, the topic reliability of the LS gains is shortly addressed.

## INTRODUCTION

SHJ cells are one of the emerging passivated contacts solar cell technologies that are in the race to become the next generation single junction cell technologies but have also a huge potential as bottom cells in silicon perovskite tandem devices [1]. Figure 1 (a) displays a sketch of a typical rear emitter SHJ cell. Lightsoaking (LS) [2-6] can have positive effects on surface passivation and the series resistance $R_s$, enables application of more transparent TCO and in combination with edge passivation allows the effective regain of cell separation losses. During application of LS the thermal budget of the complete solar cell and module process and potentially also during field exposure needs to be considered to take full advantage of the treatment. The LS treatment impacts different parts of a SHJ cell, potentially impacted parameters are $V_{oc}$ via improved passivation, change of the TCO layer optical properties, metal finger line resistance $R_{line}$, contact resistance $\rho_c$ and bulk $R_{sh}$ of the different layers and interfaces present in the SHJ cell. An overview is shown in Fig. 1 (b). The effect of LS on the passivation is often discussed in literature [2-5] where most prominent $V_{oc}$ can be boosted in the range of up to 4 mV (~0.5%$_{rel.}$). Another aspect is the reduced $R_S$ by LS which results in substantially increased FF. One part of the FF gain is associated to the improved passivation quality which results in increased $V_{oc}$. Also, at MPP this leads to increased concentration of carriers in the wafer and reduces the effective resistivity of the wafer via conductivity modulation [7]. Also, for HC cells or shingles with cut edges LS can help to improve the cell properties. The high defect density $D_{it}$ or dark saturation current $J_{02,edge}$ [8-12] at the fresh cut

*SiliconPV 2022, the 12th International Conference on Crystalline Silicon Photovoltaics*
AIP Conf. Proc. 2826, 090004-1–090004-9; https://doi.org/10.1063/5.0141313
Published by AIP Publishing. 978-0-7354-4536-9/$30.00

edge can be improved, especially if passivated edge technology (PET) is applied. For SHJ cells LS gains on cell level are widely discussed in literature while the question if this transfers from cell to module without losses is less discussed. Only recently in [13] data were reported on the impact of LS on cell and module level as well as the effect of lamination. But the question of long-term stability of LS under field conditions is not published to our knowledge, yet.

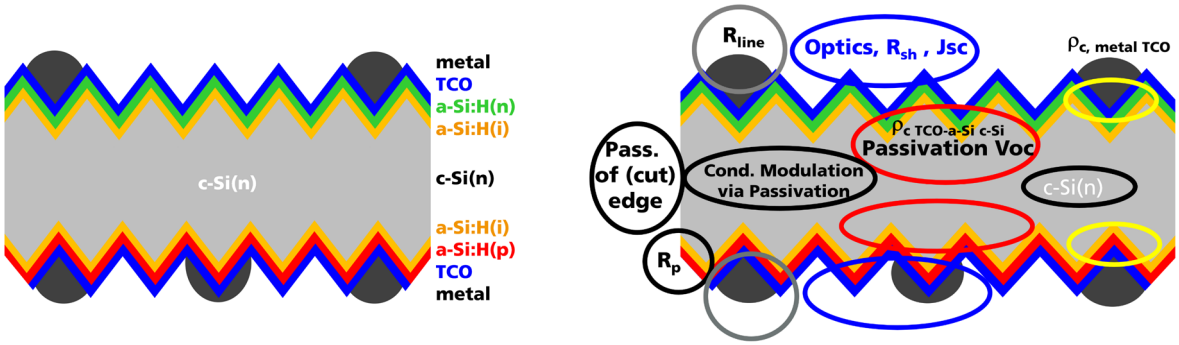


**FIGURE 1.** (a) Sketch of the rear emitter SHJ cell. (b) The different parts/parameters that might be affected by LS are marked.

## EXPERIMENTAL

Four cell batches were processed to investigate the interaction of LS with FC and HC cells. The first batch addresses the interaction of LS with TCO and the optimal choice for high η after LS. Within the second and third batch HC cells are processed. In the second batch the impact of edge passivation in the post processing procedure was tested with the focus on reducing cutting losses while in the third batch a slim post processing procedure for HC cells is addressed. These cells are subsequently integrated into modules. In the last experiment the reliability of LS on module level is investigated.

### Cell Optimization and TCO LS Interaction

Light Soaking leads to increased FF and reduced $R_S$ in SHJ solar cells. A part of this $R_S$ reduction is linked to improved passivation, but a second part originates from the change of the TCO properties that also affect lateral current transport. To investigate this effect SHJ cells with varied TCOs properties were produced. Our SHJ baseline process sequence [5] was applied for cell production where for the TCO layer deposition a SCALA tool from Von Ardenne was used. The deposition was carried out with an ITO 97:3 target and the gas flow of $H_2$ and $O_2$ was varied. The TCO was deposited symmetrical on front and rear side of the SHJ cells. After IV measurement half of the cells were exposed to rapid thermal process (RTP) laser based Light Soaking [5,6] and measured a second time. To investigate the $R_{sh}$ of the finished solar cells 1 cm wide stripes were cut for both groups and measured with TLM (transfer length method) on the pn-junction rear side.

### HC Cells with Passivated Edge

To address the losses associated with the HC cell separation a batch of SHJ full cells (FC) was produced on basis of 1 Ωcm n-type Cz M2 size wafers. The wafers were processed in the frontend by applying an alkaline texture (aTx) step, a following a-Si deposition by plasma enhanced chemical vapor deposition (PECVD) and finally a TCO deposition by physical vapor deposition (PVD). Then the cells were finished in the backend with a low temperature paste metallization on both sides including a 6BB print with continuous busbars. The cells were cured offline in a convection oven and initially measured with an automated cell tester. The FC host cells were separated in two groups with similar mean η. The first half was exposed to the laser based rapid thermal process (RTP), similar to [3-6] and measured again. The second part was cut into half cells by a thermal laser separation (TLS) process, adapted for low damage cell separation. After separation an edge passivation step (PET) was carried out and the half-cut cells (HC)

were re-measured. Finally, the HC cells were also treated with the LS process and measured again. The process sequence and sketches of LS and TLS processes are shown in Fig. 2., compare [8-10].

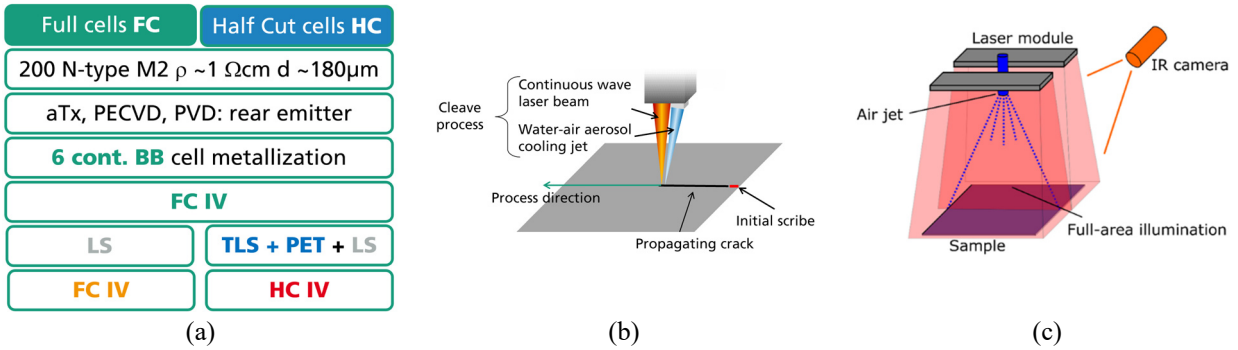


(a) (b) (c)

**FIGURE 2.** (a) Process sequence for HC cells, (b) sketch of TLS process applied for separation of HC cells [9] (c) sketch of the RTP laser based Light Soaking [6].

## HC Cells for Module Integration

In a third large batch SHJ HC cells were produced for integration in large area modules. The HC cell process sequence used in the second batch above was adapted: due to stringer availability reasons the metallization was changed to 5BB and the edge passivation step PET was omitted. After separation the cells were measured again. The process sequence is summarized in Fig. 3 (a).

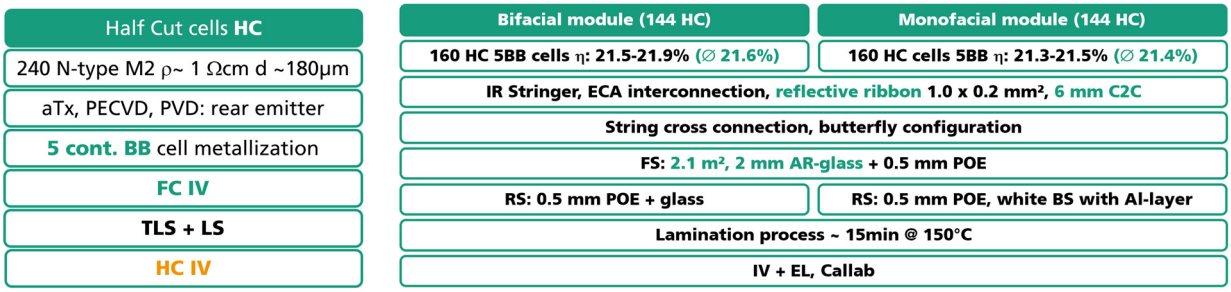


(a) (b)

**FIGURE 3.** (a) Process sequence of cell batch for HC cells and (b) integration into modules

The best 320 cells from this batch were sorted in two groups one with higher and one with lower η. These cells were then integrated into large area modules with 72 M2 FC equivalent in "butterfly" configuration [14]. One module was chosen to be in monofacial, with white backsheet (BS), and the other one in bifacial configuration. The cells with higher η were used for the bifacial module. An infrared (IR) stringer was used to glue reflective ribbons with electrically conductive adhesives (ECA) on the busbars of the cells. Cell to cell (C2C) spacing in the string was fixed to 6 mm. Per module 12 HC strings were cross connected in the butterfly configuration. For module lamination on the frontside a 2 mm anti reflective (AR) coated glass was used. The cells were laminated between two sheets of polyolefin (POE) encapsulant. After lamination the modules were characterized in the Callab by measuring the IV curves and recording EL images. The module process is shown in Fig. 3(b).

## Reliability of LS on Module Level

To address the question of long-term stability of light soaked SHJ cells mini modules were built and tested. For this test ten 5BB SHJ cells were produced and measured. This initial cell measurement represents the reference IV data point for each sample. Half of the cells were treated with LS RTP process while the other half was not exposed to LS. All cells were then measured a second time and then integrated into single cell modules. After lamination the samples were measured with a mask that covered the module outside the active cell area. To compare η of cell and mini module the median $CTM_\eta$ for non-LS cells was determined and all module η data was corrected for this $CTM_\eta$ loss. From each group (LS cells and non-LS cells) one samples was selected and stored in the dark at room temperature as reference while the four remaining mini modules per group were exposed to module light soaking (mLS) with 1000 W/m² at 75°C. The mini modules were each connected to a fixed resistance and thereby held close to the maximum power point (MPP) condition to simulate field conditions. The procedure is sketched in Fig. 4. The module samples were measured after 10, 20, 40, 80, 250, 400 and 575 h of exposure.

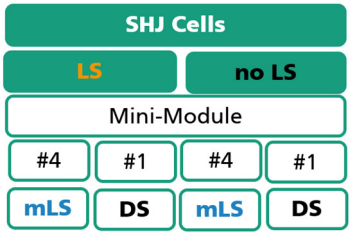


**FIGURE 4.** Sample overview for reliability of the LS gain investigation

# RESULTS ON CELL AND MODULE LEVEL

## Cell Optimization and TCO LS Interaction

The effect of LS on the sheet resistance ($R_{sh}$) determined by TLM is shown in Fig. 5 (a). Clearly the LS leads to a systematic decrease of the $R_{sh}$ in the range 7-20%. The LS shows a similar effect that is known for TCO annealing in the dark. In both cases a drop in $R_{sh}$ is found. Not shown is the TLM contact resistivity data where due to the substantial scattering a systematic impact of the LS could not be investigated. Also shown in Fig. 5 is the relative change of IV parameters in the LS process. The $V_{oc}$ and pFF changes are rather small what might be explained by the fact that before the initial IV the cells were cured inline with a combined IR + convection heating that has LS character and leads to a partial light-soaked state [15]. Nevertheless, in tendency samples with higher $R_{sh}$ show a higher gain in both parameters. The $J_{sc}$ is slightly reduced. The small difference is expected to result from measurement variability or a slight degradation of the $J_{sc}$ which might have occurred. The FF gain by LS is clearly depending on the composition of the TCO. On one hand if a high $R_{sh}$ TCO is applied (groups with 7% $O_2$) the LS reduces the $R_{sh}$ and improves the matching of the front and rear side metal pitch to the $R_{sh}$ of the TCO. On the other hand, if a low resistivity TCO (3% $O_2$) is applied, LS has a negative impact in form of FF and η degradation. As a takeaway for highest η the TCO / grid design should be optimized for high performance after LS. In this batch post curing 5% $O_2$ ITO showed the highest η, but 7% $O_2$ 0.8% $H_2$ ITO gained more in LS and had the final (post LS) highest η.

This learning together with further cell process optimizations led to an improved best full area SHJ cell processed at Fraunhofer ISE with η=23.5% after LS. For the measurement in the Callab a Grid Touch contact unit on gold chuck was used. The IV parameters of this cell are shown in Tab. 1. Metallization was not adapted for the cell GT measurement and with this the cell is module compatible. Depending on the interconnection process a second metallization step to print busbars would be necessary what would lead to a reduction of $J_{sc}$ due to shading.

**TABLE 1.** Best 0BB full area SHJ cell at Fraunhofer ISE, front contacted with Grid Touch and gold chuck rear.

| IV | Area [cm²] | $J_{sc}$ [mA/cm²] | $V_{oc}$ [mV] | FF [%] | η [%] |
|---|---|---|---|---|---|
| Callab GT+GC | 244.53 | 38.65 | 740.0 | 82.2 | **23.51** |

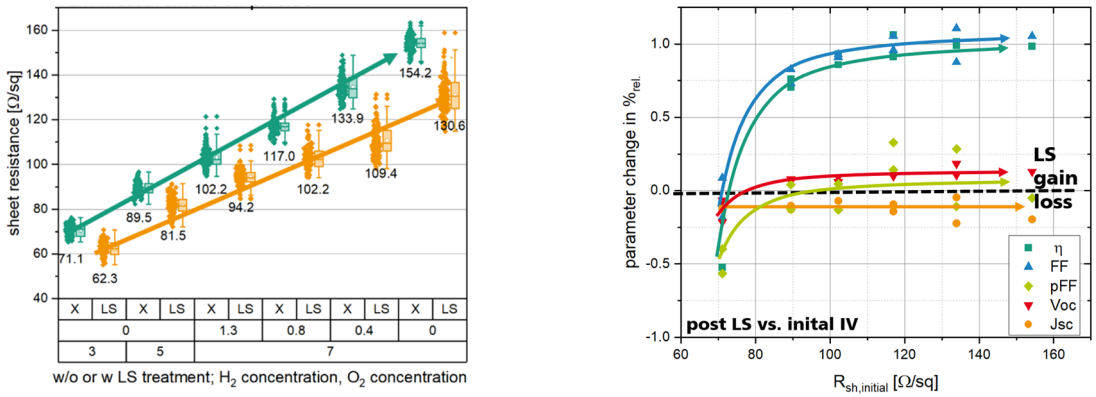


**FIGURE 5.** (a) Sheet resistance determined by TLM for ITO with $O_2$ and $H_2$ variation prior to and post LS (the relative % gas flow is shown on the x-axis). In (b) the corresponding relative IV parameter change due to the LS process is shown.

## HC Cells with Passivated Edge

The IV results for the cells during the process stages documented in the experimental part are shown in Fig. 6. During the combined separation and edge passivation step the cells lost 0.3%$_{abs.}$ in η. This loss could be overcompensated by the subsequent LS process with an η-gain of 0.5%$_{abs.}$ and with this the η-level of the LS treated HC is with about -0.1%$_{abs.}$ close to the level of the light-soaked FC that gained 0.3%$_{abs.}$ during LS. The obtained IV parameters prove the high quality of the developed post-processing procedure. Comparing the two LS (FC and HC) groups: for HC the FF is only 0.2%$_{abs.}$ lower, $R_S$ is on the same level and $V_{oc}$ is about 1 mV lower. Overall, within the scattering the FC and HC cell yield a nearly equivalent output on cell level. Both FC and HC were integrated in large area modules. Unfortunately, some cells in this batch were short circuited during the interconnection with ECA due to this the results are not representative, and we resign to show them here.

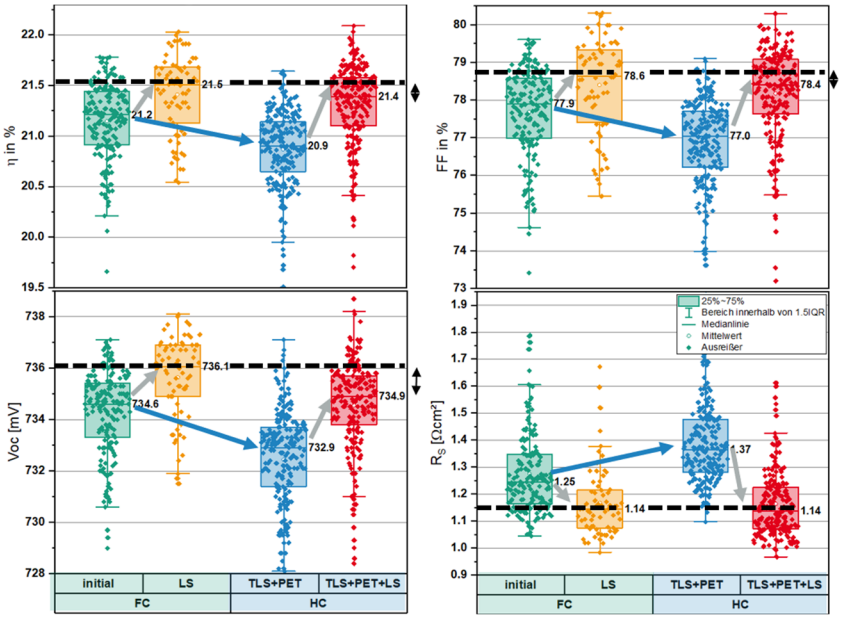


**FIGURE 6.** IV parameters of the second cell batch comparing FC before and after LS as well as cells after separation and final LS.

## HC Cells for Module Integration

For the module cell batch, the metallization was adapted from 6BB (0.5 mm) to 5BB (0.8 mm wide). This leads to an η-loss of about 0.4% $_{abs}$. for 6BB and about 0.6%$_{abs}$. for 5BB due to the BB shading. The IV results are shown in Fig. 7 (a). Comparing the partially light soaked FC and the HC after combined TLS and LS the η-loss is with < 0.1%$_{abs.}$ very small. Further comparing the IV parameters: a small loss can be attributed to the FF < 0.3%$_{abs.}$ and less than 1 mV in $V_{oc}$. The pFF degraded by 0.9%$_{abs.}$ what shows that we lost FF potential that might be recovered by applying a PET step as in the prior cell batch. In summary the slim separation process sequence worked, and the separation losses were in a reasonable range.

The 320 best HC cells were selected an integrated in two modules, each consisting of 144 HC cells. Images of the module as well as EL images are summarized in Fig. 7 b,c and d. Table 2 shows the IV data of the monofacial module together with median IV parameters of the cells that were used to make the module. The cell to module (CTM) factor is calculated for each IV parameter. For the monofacial module 400 W STC power on the frontside were measured.

**TABLE 2.** Frontside IV data of cells (median) that were used for the monofacial module and the calculated cell to module factor.

| Sample | IV | $I_{sc}$ [A] | $V_{oc}$ [V] | $P_{mpp}$ [W] | FF in % | η in % | p [W/m²] |
|---|---|---|---|---|---|---|---|
| cells | CT FS | 4.5 | 0.733 | 2.61 | 79.4 | 21.4 | 214 |
| module | FS | 9.6 | 53.1 | **400.4** | 78.8 | 19.1 | 191 |
| CTM | | **106.6%** | 100.5% | **106.3%** | **99.3%** | 89.1% | 89.1% |

Compared to the median cell power the module power was increased by about 6%$_{rel}$. This power gain is dominated by $I_{sc}$ gains that can be explained by the following factors.

- Large cell to cell spacing with reflection gains from the white backsheet in the area between the cells.
- The cells were initially measured with black chuck calibration. In the module the white backsheet behind the cells reflects a large amount of the IR photons that pass through the bifacial cell. These photons are partially absorbed and in consequence increase the current.
- The TCO on the FS of the SHJ cells has a high absorption in the UV-blue range. This leads to lower $I_{sc}$ of SHJ cells measured in air but since the glass and encapsulation in the module also absorbs significantly in this wavelength region the $I_{sc}$ of SHJ cell suffers less compared to cells with improved UV-blue response when integrated into a module. This leads to a reduction of the $CTM_{Isc}$ loss.
- For metallization five continuous busbars were printed on the cells. These lead to shading in the IV measurement of the cells. The current of the cell is reduced. In the module this busbar area is covered by the ribbon. Additional shading due to active cell area covered by the ribbon is reduced.
- For these modules reflective ribbons were used that allow improved reflection gains in the ribbon area.

For the bifacial module, made from the higher efficient cells, the IV data is summarized in table 3. Here 387 W STC power were measured for the front side. The CTM is with 102% for a bifacial module comparatively high. Comparing the two modules the one with backsheet leads to about 5% higher current in the monofacial case. Due to the HC design and the reduced cell current of the cells the FF-losses for the bifacial module are only 0.3%$_{rel.}$. The bifacial module was measured also from the rear side. With the back to front ratio (BFR) the relative to front side performance is calculated for each IV parameter. The data is shown in table 4. With a BFR > 90 % SHJ bifacial modules show a high performance in high albedo environments. About 5% contribution from the rear leads to similar performance compared to the monofacial module and with higher rear side contribution the power density rises further enabling higher yields in field for high albedo surroundings.

**TABLE 3.** Frontside IV data of cells (median) that were used for the bifacial module and the calculated cell to module factor.

| Sample | IV | $I_{sc}$ [A] | $V_{oc}$ [V] | $P_{mpp}$ [W] | FF in % | η in % | p [W/m²] |
|---|---|---|---|---|---|---|---|
| cells | CT FS | 4.5 | 0.735 | 2.64 | 80.0 | 21.6 | 216 |
| module | FS | 9.1 | 53.2 | **387.4** | 79.8 | 18.4 | 185 |
| CTM | | **101.6%** | 100.5% | **101.9%** | **99.7%** | 85.4% | 85.4% |

**TABLE 4.** Frontside and rear side IV data of the bifacial module. From these two measurements the back to front ratio (BFR) is calculated.

| Sample | IV | $I_{sc}$ [A] | $V_{oc}$ [V] | $P_{mpp}$ [W] | FF in % | η in % | p [W/m²] |
|---|---|---|---|---|---|---|---|
| module | FS | 9.1 | 53.2 | **387.4** | 79.8 | 18.4 | 185 |
| module | RS | 8.3 | 53.1 | **353.1** | 80.7 | 16.8 | 168 |
| BFR | | 90.3% | 99.7% | **91.1%** | 101.2% | 91.1% | 91.1% |

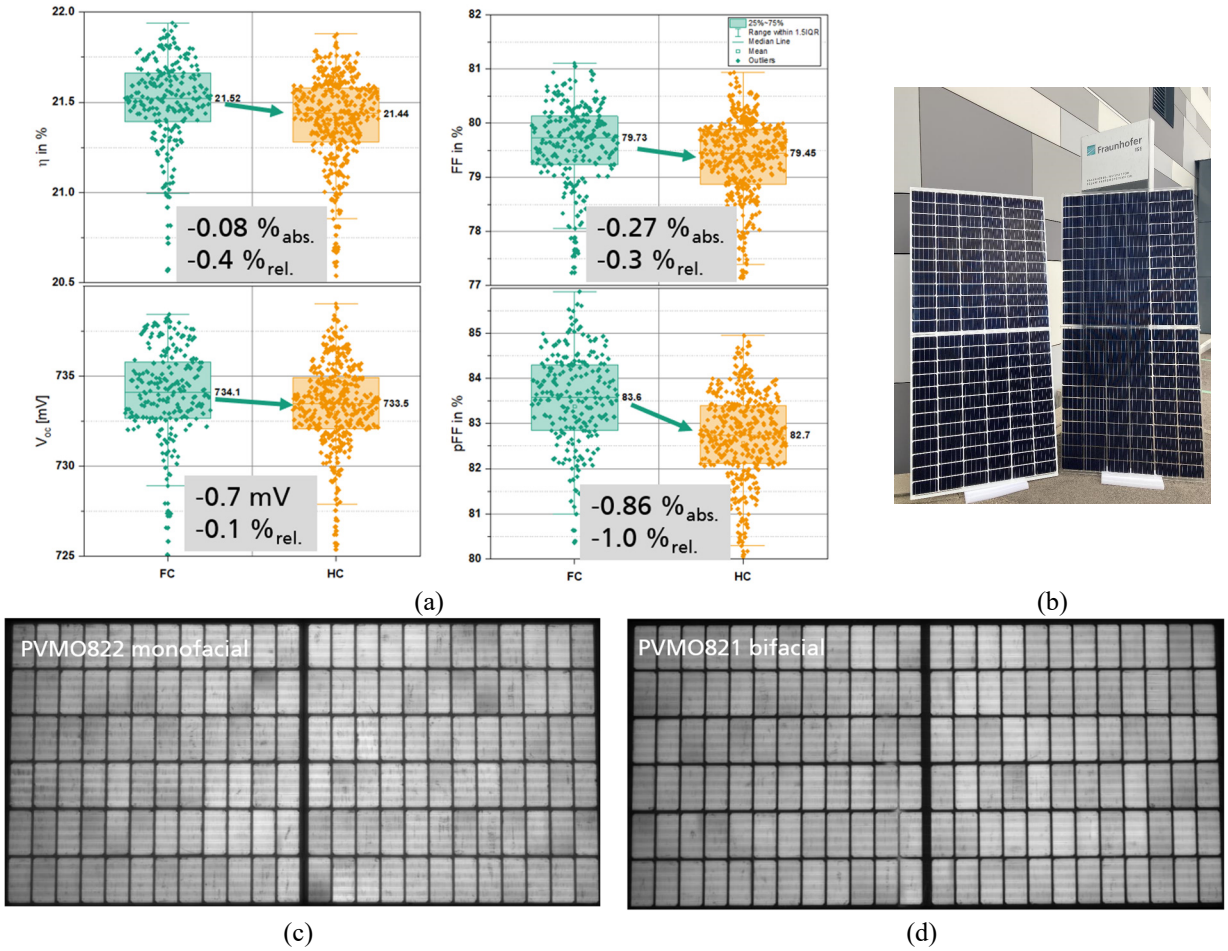


**FIGURE 7.** (a) IV parameter recorded during HC process sequence for module integration, (b) photograph of the monofacial (left) and bifacial (right) module and in (c) and (d) the EL images of the monofacial and bifacial module.

## Reliability of LS on Module Level

In the LS step on cell level the gain was in median 1.8%$_{rel.}$ in η compared to initial cell measurement. The non-LS cells showed minor change in η. This might be explained by measurement uncertainty or a slight degradation of the sample. This first data point in Fig. 8 represents the initial LS gain on cell level. The second data point represents the initial values for the modules corrected for the $CTM_{\eta}$ of non-LS cells, as described in the experimental section. The following data points show the relative η change after exposure to light in the module LS (mLS) or module dark storage (DS). For the DS samples a minor change during the 575 h exposure can be seen, slight negative trend but all <0.5%$_{rel.}$ in η. The mLS group show an improvement in the η by about 0.5%$_{rel.}$ for modules with pre-LS cells and with 0.8 %$_{rel.}$ slightly higher for the modules with non-LS cells. This peak of efficiency is found after 10 h of continuous light exposure. For the later readouts a "plateau" is found in the range 10 to 40 h then for prolonged testing a

degradation was detected for both groups. The pre-LS group degrades by 1.7%$_{rel.}$ while the non-pre-LS group degrades by 1%$_{rel.}$. Both groups degrade clearly below the found peak after 10 h of mLS but also below the η after lamination. In literature LS issues are describe in case of insufficient doping or layer thickness on the p-side [16]. Here further degradation studies are needed to investigate if there is optimization potential available in mLS stability of SHJ modules.

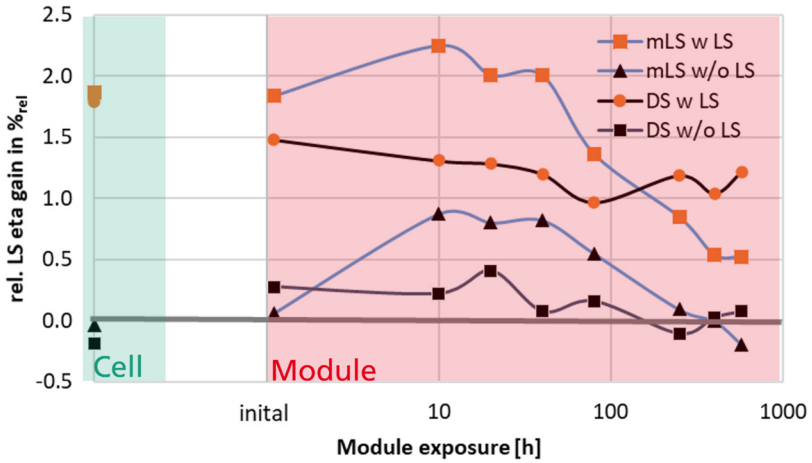


**FIGURE 8.** Evolution of the LS η-gains on cell and module level. For comparison also the references stored in the dark are shown.

## SUMMARY AND CONCLUSION

In this work relevant topics for SHJ cell and module integration were addressed. These are cell cutting and LS, interaction of LS with TCO and reliability of LS gain in module and long-term light exposure. Results from a low loss or even lossless cell separation process for a large 6BB cell batch were shown. The process sequence TLS+PET+LS allows to reach even higher η after separation compared to the initial measurement of the host cell. If compared to the light-soaked host cell the loss for the HC sequence is with 0.1%$_{abs.}$ low. This enables application of HC process route where the benefits from HC cell module integration clearly surpass the η-change due to the separation sequence. In another cell batch 5BB HC cells were produced with the sequence TLS+LS omitting the edge passivation process. Compared to the non-light-soaked host FC an η-loss < 0.1%$_{abs.}$ was found. From this cell batch two 144 HC cell modules were built, and the IV data was presented. The monofacial module surpassed 400 W with a CTM$_{Pmpp}$ of 106% while the bifacial module achieved 387 W with a CTM$_{Pmpp}$ of 102% and the BFR >90% what enables higher power densities in the field if the Albedo of the background allows a significant contribution from the rear side.

Also discussed were the results from a cell batch with varied ITO symmetrically deposited on front and rear side of SHJ cells. The LS gain was found to depend on the initial sheet resistance of the TCO. Samples with initial $R_{sh}$ of 90 Ω/□ on both sides performed best after curing while after LS the group with about 120 Ω/□ performed best. This experiment shows that optimizing the cells for post LS enables higher η. This learning together with further process optimizations were implemented in the SHJ baseline at Fraunhofer ISE and recently an η of 23.5% was achieved for a full area busbar less cell post LS measured with Grid Touch on a gold chuck in the Callab.

In the last part of this work results from an experiment addressing the long-term reliability of LS gain were discussed. LS gains on cell level could be transferred from cell to module. Subsequent long term module LS in MPP condition lead for mini modules in the first few hours of exposure to η-gains but in the longer run these gains degraded and the results after almost 600h of exposure were close to the initial cell results before LS. These findings show the importance of further research and development in long-term stability of SHJ in general but especially the effect of managing the thermal budget along the process chain also for additional process steps like LS.

## AKNOWLEGEMENTS

We would like to thank the Federal Ministry of Economic Affairs and Climate Action for funding in the DYNASTO project (FKZ 0324293A) in which the TCO investigation were done. Furthermore, we would like to thank our colleagues from the departments QCS, POG, PSM, PVM, AMK at Fraunhofer ISE for their support of this work. Alexander Krieg and Jan Löffler for measuring solar cells with high accuracy in the automated cell tester. Fiona Hatzelmann and Johannes Greulich for contributing with TLM measurements and result discussion. Jonas Stegmaier, Heike Brinckheger and Katrin Krieg for taking care about the wet chemistry processes. Diana Witt, Milad Salimi Sabet, Marc Retzlaff, Michael Linse, Pedro Sansoldo, Nómar Cárdenas, Dilara Kurt, Homeira Hashemi, Ikram Eloudjeditalet, Lisbeth Andrea Rangel Herrera for (post-)processing in PVTEC front- and backend.

## REFERENCES

1. C. Messmer et al., “The race for the best silicon bottom cell: Efficiency and cost evaluation of perovskite–silicon tandem solar cells” PiP (2020)
2. E. Kobayashi et al., “Light-induced performance increase of silicon heterojunction solar cells,” Appl. Phys. Lett., vol. 109, no. 15 (2016)
3. B. Hallam et al., “Defect-Engineered Silicon Heterojunction Solar Cells”, Chengdu, China, Nov. 18, 2019.
4. M. Wright et al., “Progress with Defect Engineering in Silicon Heterojunction Solar Cells”, Phys. Status Solidi RRL 2021, 15, 2100170
5. A. Moldovan et al., “Improved Layer Properties combined with Light Soaking enabling for 23% efficient silicon heterojunction solar cells”, EUPVSEC (2020)
6. S. Roder et al., “High-Intensity Light Soaking Treatment of Silicon Heterojunction Solar Cells: Process Development and Inline Transfer”, EUPVSEC (2021)
7. J. Haschke et al.,” Lateral transport in silicon solar cells”, JAP (2020)
8. P. Baliozian et al., “Postmetallization “Passivated Edge Technology” for Separated Silicon Solar Cells”, IEEE J. Photovolt., vol. 10, no. 2 (2020)
9. P. Baliozian et al., “Thermal laser separation of PERC and SHJ solar cells” IEEE J. Photovolt., vol. 11, no. 2 (2021)
10. A. Münzer et al., “Postseparation Processing for Silicon Heterojunction Half-Solar Cells with Passivated Edges” IEEE J. Photovolt., vol. 11, no. 6 (2021)
11. B. Portaluppi et al., “Insights on cell edge defects impact and post-process repassivation for heterojunction”, EUPVSEC (2020)
12. A. Fell et al., “Modeling Edge Recombination in Silicon Solar Cells”, IEEE J. Photovolt., vol. 8, no. 2 (2018)
13. J. Cattin et al., “Transferability of the light-soaking benefits on silicon heterojunction cells to module”, submitted to IEEE (2021)
14. N. Klasen et al., “Quantitative Evaluation of the Shading Resilience of PV Modules”, EUPVSEC (2021)
15. D. Erath et al., “Fast Screen Printing and Curing Process for Silicon Heterojunction Solar Cells”, Metallization Workshop (2020)
16. J. Cattin et al., “Influence of Light Soaking on Silicon Heterojunction Solar Cells with Various Architectures”, IEEE J. Photovolt., vol. 11, no. 3 (2021)